JCTC Journal of Chemical Theory and Computation

Force Field Effects on a β-Sheet Protein Domain Structure in Thermal Unfolding Simulations

Ting Wang* and Rebecca C. Wade

Molecular and Cellular Modeling Group, EML Research, Schloss-Wolfsbrunnenweg 33, 69118 Heidelberg, Germany

Received June 22, 2005

Abstract: The secondary structure propensities observed in protein simulations depend heavily on the force field parameters used. The existing empirical force fields often have difficulty in balancing the relative stabilities of helical and extended conformations. The resultant secondary structure bias may not be apparent in short simulations at room temperature starting from the native folded states. However, it can manifest itself dramatically at high temperatures and lead to large deviations from experimentally observed secondary structure propensities. Motivated by thermal unfolding simulations of several WW domains, which have a three-stranded β-sheet structure, we chose the FBP28 WW domain as a well-characterized system to investigate several AMBER force fields as well as parametrization of the NPSA (Neutralized, Polarized ionizable side chains with a solvent-accessible Surface Area-dependent term) implicit solvent model. The ff94 force field and two variants with altered parameters for the backbone torsion term were found to convert the native β-sheet structure directly to a single helix at high temperatures, whereas the ff96 force field produced significant non-native β-sheet content at high temperatures. The ff03 force field was able to reproduce the β-sheet-coil transition and experimentally observed unfolding pathways with both an explicit water solvent and the NPSA implicit solvent model at relatively low temperatures. However, the protein domain became predominantly helical after unfolding. Modification of the solvation parameter in the NPSA implicit solvent model was not sufficient to remedy this problem. The results imply that the intrinsic secondary structure bias in a force field cannot easily be solved by modifying a single parameter such as backbone torsion potential or a solvation parameter of a solvent model. Nevertheless, the results show that the AMBER ff03 force field together with an explicit solvent model or the NPSA implicit solvent model is a useful tool for studying the unfolding of both α- and β-sheet structure protein domains, and an integrative consideration of all force field parameters is likely to be necessary for a complete solution.

Introduction

Empirical molecular mechanics force field parameters are generally used for macromolecular modeling and simulation due to the unaffordable computational cost of performing ab initio quantum mechanics calculations. Widely used molecular mechanics force fields include AMBER,[1−4] CHARMM,[5,6] GROMOS,[7] and OPLS.[8] These force fields produce reasonable results for many studies. However, because empirical force fields are parametrized by fitting to experimental results and ab initio quantum mechanics calculations for a limited number of small peptides or nucleotides, difficulties exist when the parameters are applied to proteins and nucleic acids. For this reason, force fields are continually being improved on the basis of the increasing understanding of proteins and nucleic acids and advances in computational methodology and computer power. For example, the AMBER force field has developed from ff94,[1] ff96,[2] and ff99[3] to the current ff03.[4] In simulations of

* Corresponding author e-mail: ting.wang@eml-r.villa-bosch.de.

10.1021/ct0501607 CCC: $33.50
Published on Web 12/08/2005

dynamic processes such as protein folding, unfolding, and flexible docking, the accurate treatment of protein conformations and interactions is crucial. This requires accurate parameters for both helical conformations and extended conformations. Helical conformations are strongly dependent on local interactions, e.g. i, i+4 hydrogen-bonding interactions in the α-helix, whereas β-sheet conformations are more influenced by nonlocal (in sequence) interactions. Thus, it is more difficult to model β-sheets. In addition, most of the model peptide systems used to derive force field parameters, such as polyalanine peptides, are systems that preferentially sample helix-coil conformational space. As a consequence, the existing force fields often show a bias toward overstabilizing α-helical and understabilizing β-extended conformations.[2,4,9−15] Many parameters can affect protein conformations, including atomic charges, nonbonded interaction parameters, and backbone torsion (ϕ and φ) angle parameters. Among these, backbone torsion (ϕ and φ) angle parameters are the most directly related to protein secondary structure formation and therefore often used to adjust the secondary structure propensity of a force field. A number of force field evaluations have been conducted by Garcia's group[10,13] and Pande's group.[11,16] The model peptides studied were helix-coil transition systems, and helical propensity was the main concern. A short 12-residue β-hairpin tryptophan zipper was studied by Simmerling and co-workers[15] to evaluate the AMBER ff94 and ff99 force fields, and the peptide was found to convert to a stable α-helix at 550 K with both ff94 and ff99 force fields. Here, we evaluate the AMBER force fields by simulation of a 3-stranded β-sheet protein domain to investigate the relative stability and the balance between helical and extended conformations. As far as we know, this investigation of the secondary structural conformational preferences of different force fields is the first based on a protein system that undergoes β-sheet-coil transitions.

This paper was initiated by our study of the relative stability of WW domains and their mutants by thermal unfolding simulations carried out with AMBER force fields and our NPSA (Neutralized, Polarized ionizable side chains with a solvent-accessible Surface Area-dependent term) implicit solvent model.[17] WW domains are small 3-stranded β-sheet protein domains with two signature tryptophan (W) residues. Extensive experiments have shown that WW domains undergo a β-sheet-coil transition upon unfolding.[18−22] However, in our early simulations with the AMBER ff94 force field, we observed that the β-strands converted into α-helices during high temperature simulations, independent of the WW domain sequence. This result prompted us to investigate the available AMBER force fields and compare their performance in terms of unfolding behavior. Because of this motivation, most simulations in this study are conducted at high temperature to enable unfolding to occur on computationally accessible time scale. Most of simulations are conducted for the FBP28 WW domain, a WW domain with an experimentally well-defined structure and comparatively high thermal stability. The folding/unfolding of this domain has been extensively studied by NMR and CD spectroscopy.[18−22] The third strand was observed to be less stable than the first two strands and to be lost first upon unfolding. The folding/unfolding of FBP28 was observed to be three-state.

Another motivation for this paper is concerned with solvent models. Previous studies revealing the helix-favoring bias in the AMBER ff94 and ff99 force fields and the extended-favoring bias in the AMBER ff96 force field were done using an explicit solvent model[10,11,13,16,23,24] or the generalized Born implicit solvent model.[9,23] In this paper, we also investigate use of our NPSA implicit solvent model,[17] which is computationally advantageous compared to both the generalized Born model and an explicit solvent model and gives good results compared to other implicit solvent models in simulations of a variety of proteins at 300 K.[17] Therefore, the evaluation of the ff94 and ff96 force fields was conducted with the NPSA implicit solvent model only. For the newer ff03 force field, we performed simulations with both the NPSA implicit solvent model and an explicit solvent model.

Materials and Methods

The FBP28 WW domain folds into a twisted three-stranded antiparallel β-sheet structure with a melting temperature of 64 °C (337 K).[22] In this study, we used the first structure in the NMR ensemble (PDB entry 1e0l) of FBP28 WW domain. It has 37 residues.

NPSA Model. The simulations of FBP28 were carried out by using the AMBER7 program, modified to incorporate the NPSA implicit solvent model. The NPSA model has been demonstrated to be efficient for maintaining protein native structures and flexibly docking proteins at 300 K.[17] The model uses a distance-dependent dielectric function ($\epsilon = r$), but the partial charges of the ionized side-chains (residues Glu, Asp, Lys, and Arg) and the N- and C-termini are neutralized (N) and polarized (P), and a solvent-accessible surface area (SA)-dependent term ($\Delta G = \sum \sigma A$) is added. The modified charges (called NPSA charges) were parametrized based on the AMBER ff94 force field. The solvation parameter σ was set as 0.012 kcal/mol·Å^2 for nonpolar carbon and sulfur atoms and −0.06 kcal/mol·Å^2 for polar nitrogen and oxygen atoms.

For the ff03 force field, we reparametrized the NPSA charges for use with the new atomic partial charges in ff03 (see Table 1). With ff03, two different values of the solvation parameter σ for backbone nitrogen atoms, −0.06 and −0.12 kcal/mol·Å^2, were tested and compared while retaining 0.012 kcal/mol·Å^2 for nonpolar carbon and sulfur atoms and −0.06 kcal/mol·Å^2 for polar oxygen atoms and side chain nitrogen atoms.

Backbone Torsion Parameters. In addition to the standard ff94, we have studied four variants with altered backbone torsion parameters: ff96,[2] Simmerling's parameters,[9] Garcia's parameters,[10] and the ff03 ϕ/φ parameters. The backbone torsion potentials (C−N−CA−C (ϕ) and N−CA−C−N (φ)) studied are plotted in Figure 1, except for Garcia's parameters in which the backbone torsion potential is set to zero. Peptide ϕ/φ dihedral angle energy terms are generally represented by a Fourier series of cosine functions that contribute additively in a force field. Modifications take place in the coefficients and phases of the cosine functions. From the plots in Figure 1, we can see that in

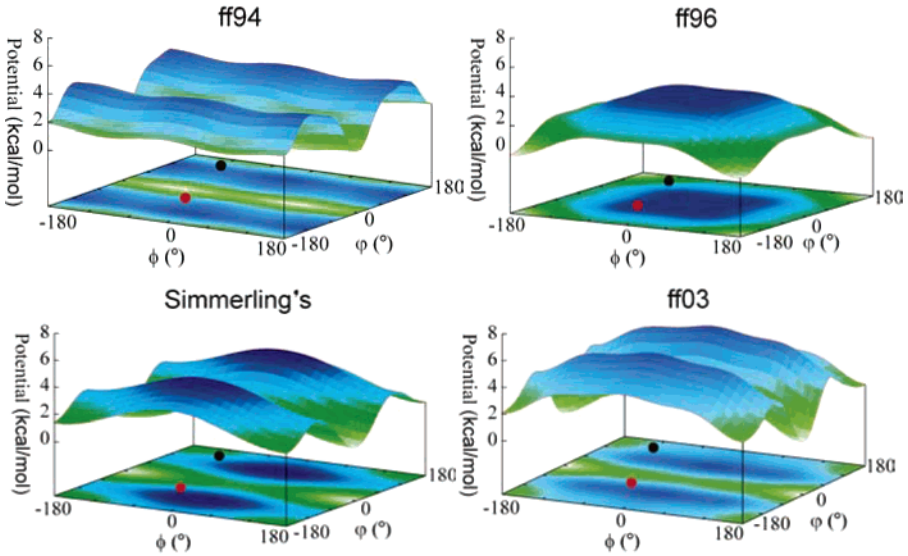

Figure 1. The backbone torsion potentials (C−N−CA−C (ϕ) and N−CA−C−N (φ)) studied in this paper, include ff94,[1] ff96,[2] Simmerling's,[9] Garcia's,[10] and the ff03[4] force field. The backbone torsion potential is set to zero in Garcia's modification and is therefore not plotted in this figure. The red dots indicate the helical conformations ((ϕ,φ) = (−60°, −40°)), and the black dots indicate β-extended conformations ((ϕ,φ) = (−120°, 140°)). In ff94, the helical regions are closer to the energy minimum than extended regions, whereas in ff96, helical regions lie on the energy maximum. In Simmerling's modification and ff03, both helical and extended conformations are located intermediates between the energy minimum and maxima.

Table 1. Modified Partial Atomic Charges (e) for Ionized Side Chains and the N- and C-Termini Used in the NPSA Model Based on the ff03 AMBER Force Field[c]

	ASP		GLU		LYS		ARG	
ionizable side chains	CG	1.3452	CD	1.3652	NZ	−1.4504	NH1,2	−0.7858
	OD1,2	−0.5804	OE1,2	−0.6740	HZ1,2,3	0.3946	HH1,2,3,4	0.3411
	CB	0.0519	CG	0.0659	CE	−0.1698	CZ	0.0655
							HE	0.2262
NTER[a]	H = original charge + 0.1							
	N = original charge − 1.3							
CTER[b]	O = original charge + 0.2							
	C = original charge + 0.6							

[a,b] In the AMBER force field, the charges of the side chain atoms of ASP, GLU, LYS, and ARG are slightly different when they are terminal residues. The modified charges of the side chains of these terminal residues are therefore slightly different from those listed above but were assigned by following the same logic as in the reference paper.[17] The full list of NPSA partial atomic charges is available in the Supporting Information. [c] The side chains are neutralized and polarized in the NPSA model.

ff94, helical regions are closer to the energy minimum than extended regions, whereas in ff96, helical regions lie on the energy maximum. In both Simmerling's modification and ff03, helical and extended regions are located intermediate between the energy minimum and maxima.

Simulation Protocol. In simulations with the NPSA implicit solvent model, the structures of FBP28 were first energy minimized for 200 steps and then gradually heated from 0 K to the desired temperatures in 50 ps. They were then simulated at that temperature with a temperature-coupling constant of 1.0 ps. The bonds involving hydrogen atoms were constrained by using the SHAKE algorithm. A time step of 2 fs was used, and the nonbonded interactions were updated every 10 time steps with a cutoff of 10 Å.

In simulations with an explicit water model, the structure of FBP28 was solvated in a truncated octahedron TIP3P water box with a minimal distance of 12.0 Å between the boundaries of the box and the nearest protein atoms. 4391 water molecules were added to the system. The water molecules were subjected to 2000 steps of energy minimization, and then the whole system was energy minimized for 1000 steps. After energy minimization, the whole system was subjected to a gradual heating from 0 K to the desired temperature in 50 ps and kept at that temperature with a temperature coupling constant of 1.0 ps. The bonds involving hydrogen atoms were constrained by using the SHAKE algorithm. The time step was 2 fs, and the nonbonded interactions were updated every 10 time steps with a cutoff of 10 Å. The Particle Mesh Ewald (PME) method was used for the long-range electrostatic interactions with the default parameters. Constant volume was used in the first 300 ps, and a constant pressure of 1.0 atm was used for the rest of the simulation time.

The secondary structure element assignment was calculated with the program STRIDE[25] embedded in the software VMD 1.8.3.[26]

Results and Discussion

ff94, ff96. FBP28 was first simulated with the ff94 force field and the original NPSA parameters at 430 K. The

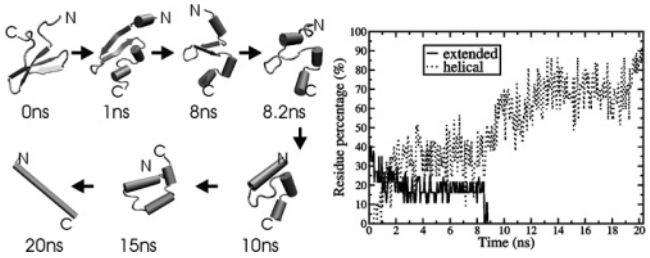

Figure 2. The 3-stranded β-sheet native structure of FBP28 gradually converted to a single helix when simulated at 430 K with the NPSA model and the ff94 force field. The right-hand plot shows the time development of the percentage of residues in extended (solid line) and helical (dash line) conformations. Significant helices appeared after ca. 1 ns and continued growing to occupy the whole protein. There was not even transient loss of helical content.

simulation temperature 430 K is higher than the melting temperature of FBP28 (337 K[18,22]), and the native 3-stranded β-sheet structure was indeed lost. However, the protein did not change to a random coil structure but gradually and directly converted to a single helix in 20 ns as shown in Figure 2. The plot in Figure 2 shows the time development of the percentage of residues in extended (solid line) and helical (dash line) conformations. Significant helices appeared after ca. 1 ns and continued increasing to occupy the whole protein. There was not even a transient coil state between the initial β-sheet structure and the final α-helix structure. This result is in disagreement with experiments[18−22] where no structured protein was observed in the unfolded states. The helical content of FBP28 was predicted to be 0.75% and 0% by the program Agadir[27] and the Web server PredictProtein,[28] respectively. The overstabilization of helix is apparent.

With respect to the unfolding pathway, the first two strands were much more persistent than the third strand, and this yielded a constant percentage of residues in extended conformations between 1 ns and 8 ns in the plot in Figure 2. This is in agreement with the order of loss of β-strands observed in unfolding experiments. Importantly, regardless of the helical content, the long time persistence of the first two strands implies an intermediate between folded and unfolded states, which is consistent with the 3-state unfolding behavior observed in experiments[22] and previous unfolding simulations of FBP28 WW domain with explicit water solvent.[21] Nevertheless, the substantial helical content prevented the observation of a realistic unfolding pathway.

Several studies have reported that, by modifying backbone torsion parameters, α-helix propensity can be reduced to approach experimental values.[3,9,10,15] These studies were however based on α-helix-coil systems not β-sheet-coil systems. We tried two of the backbone torsion parameter variants[9,10,15] suggested by Simmerling and co-workers[9] and by Garcia and co-workers,[10] respectively. The backbone torsion potential with Simmerling's parameters can be seen in Figure 1; both helical and extended regions lie between the energy minimum and maxima. Garcia's modification entails simply zeroing out the backbone torsion potential. Figure 3 shows the time development of the percentage of residues in extended (left) and helical (right) conformations with different backbone torsion parameters (ϕ/φ) applied to the ff94 force field together with the original NPSA implicit solvent model at 430 K. The 3-stranded β-sheet native structure ultimately converted to single helices in all simulations although with different conversion speeds. The simulations with the four different backbone torsion parameters yielded very similar profiles of the time development of the percentage of residues in extended and helical conformations. This result indicates that, in the context of the ff94 force field, these modifications of backbone torsion parameters alone cannot rectify the overstabilization of helical conformations.

However, the situation changed dramatically when we switched to the ff96 force field, which differs from ff94 only in the backbone torsion parameters. They were reparametrized to improve the stability of β-extended structures.[2] In Figure 1, we can see that helical regions lie on the energy maximum in the backbone torsion potential in the ff96 force field. In the simulations with ff96, the 3-stranded β-sheet of FBP28 was very stable, and complete unfolding occurred only at a highly elevated temperature of 600 K. Figure 4

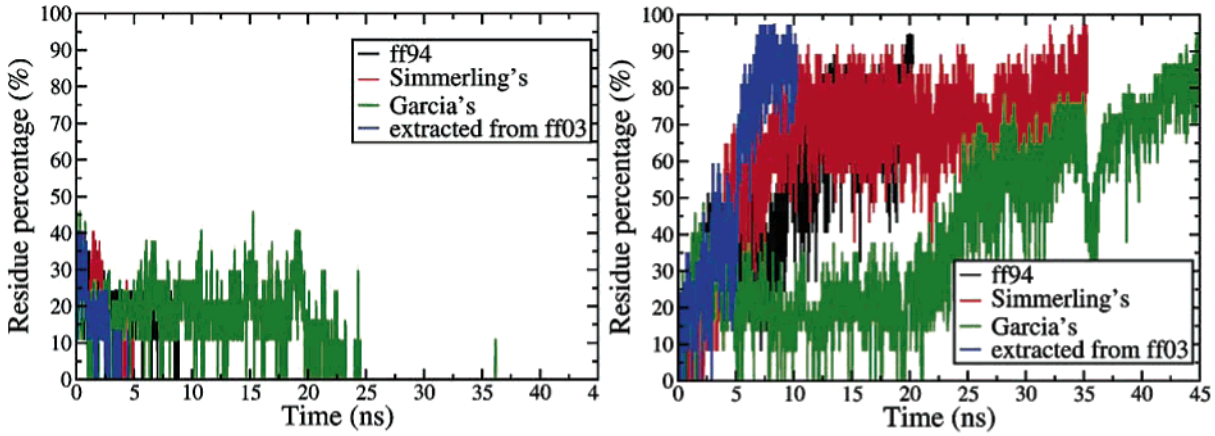

Figure 3. Time development of the percentage of residues in extended (left) and helical (right) conformations in the simulations of FBP28 with different backbone torsion parameters (ϕ/φ) applied to the ff94 force field together with the NPSA implicit solvent model at 430 K. black: ff94; red: Simmerling's; green: Garcia's; blue: (ϕ/φ) parameters extracted from ff03. The 3-stranded β-sheet native structure ultimately converted to single helices in all simulations although with different conversion speeds.

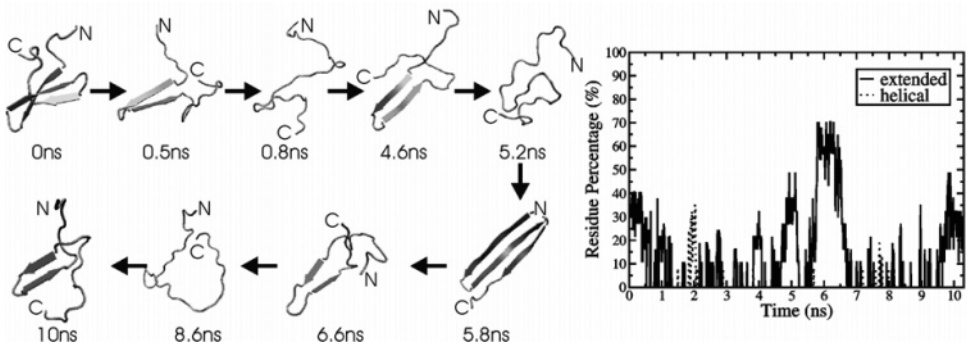

Figure 4. Representative structures of FBP28 in a 10-ns simulation with the NPSA model and the ff96 force field at 600 K. The right-hand plot shows the time development of the percentage of residues in extended (solid line) and helical (dash line) conformations. The 3-stranded β-sheet native structure unfolded in the first 1.3 ns and afterward non-native β-sheet structures appeared as the main populations. From 5.8 ns to 6.5 ns the whole structure became a long 3-stranded β-sheet. Only negligible transient helical conformations appeared.

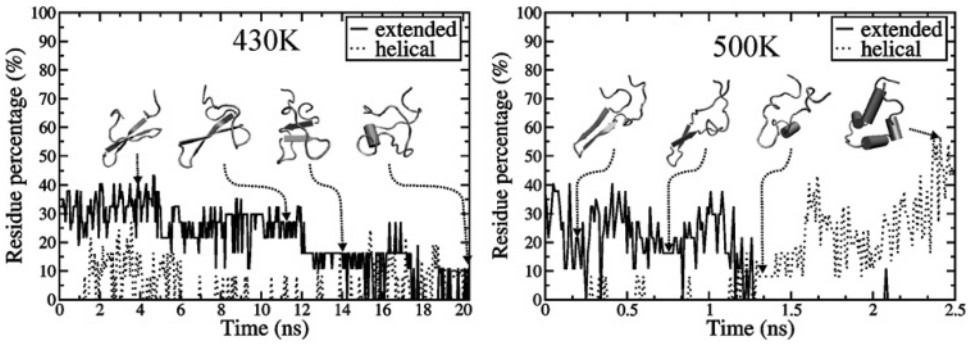

Figure 5. Time development of the percentage of residues in extended (solid line) and helical (dash line) conformations in the simulations of FBP28 with the NPSA model and the ff03 force field at 430 K (left) and 500 K (right). Although notable helical conformations are present in the trajectories, they are discontinuous until unfolding completed, losing all strands. In the left plot at 430 K, the time development of the percentage of extended conformations exhibits three steps: (1) the full the native 3-stranded structure (ca. 0−5 ns), (2) the full maintenance of the first two strands and the absence of the third strand (ca. 5−12 ns), and (3) the partial maintenance of the first two strands (ca. 12−18 ns). This enabled the observation of a clear unfolding pathway: the early loss of the third strand followed by the loss of the first two strands.

shows the representative structures of FBP28 in a 10-ns simulation at 600 K and the time development of the percentage of residues in extended (solid line) and helical (dash line) conformations. The 3-stranded β-sheet native structure unfolded in the first 1.3 ns, and afterward non-native β-sheet structures appeared as the main populations. From 5.8 ns to 6.5 ns, the whole structure became a long 3-stranded β-sheet. Only negligible transient helical conformations appeared. This result indicates the overstabilization of extended conformations in the ff96 force field, as observed in other studies using an explicit solvent model.[16,24] Although very short, the first 1.3 ns of the trajectory of FBP28 exhibited the unfolding pathway observed in experiments,[21] that is the early loss of the third strand followed by the loss of the first two strands.

ff03. With the recent distribution of the AMBER8.0 program, the ff03 force field[4] became available. The differences between ff03 and ff94 are in the atomic partial charges and backbone torsion parameters. The backbone torsion potential plot in Figure 1 shows that both helical and extended regions lie intermediate between the energy minimum and maxima.

We reparametrized our NPSA charges to be consistent with the new partial atomic charges. See Table 1 for the new NPSA charges. We conducted simulations for FBP28 at three different temperatures: 370 K, 430 K, and 500 K. At each temperature, three 20-ns runs were performed with different heating speeds to the desired temperature. At 370 K, the three-stranded β-sheet structure was stable and conserved throughout the three 20-ns simulations.

At 430 K, the structure partially unfolded during one of the three 20-ns simulations with the third strand swinging out first and then the first two strands separating. Complete unfolding occurred in the other two 20-ns simulations. The left-hand plot in Figure 5 shows the time development of the percentage of residues in extended (solid line) and helical (dash line) conformations in one of the two complete unfolding simulations at 430 K. Although notable helical conformations were still present in the trajectories, they were discontinuous until unfolding completed and all strands were lost. The time development of the percentage of residues in extended conformations exhibits three steps: (1) the full native 3-stranded structure (ca. 0−5 ns), (2) the full maintenance of the first two strands with the absence of the third strand (ca. 5−12 ns), and (3) the partial maintenance of the first two strands (ca. 12−18 ns). The last two steps together imply an intermediate between the folded and unfolded states, which is consistent with the 3-state unfolding

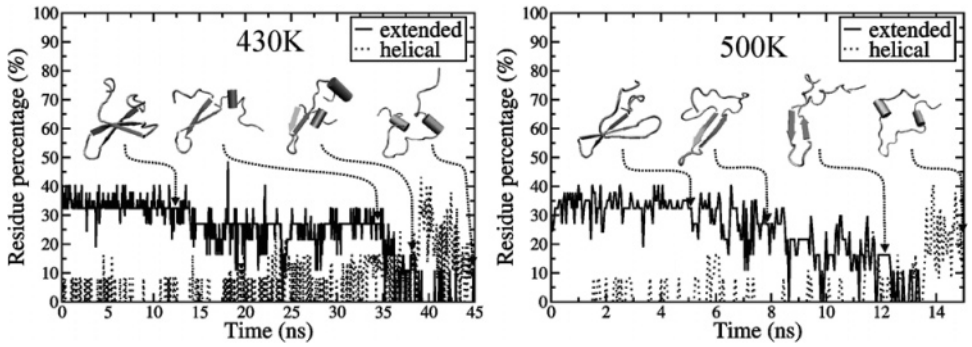

Figure 6. Time development of the percentage of residues in extended (solid line) and helical (dash line) conformations in the simulations of FBP28 with an explicit water solvent and the ff03 force field at 430 K (left) and 500 K (right). Similar to Figure 5 from the implicit NPSA solvent model, notable helical conformations are present in the trajectories but discontinuous until after complete unfolding. After unfolding, helices are the main secondary structure population. Another similarity between Figures 6 and 5 is that the unfolding pathway is clearer at 430 K than at 500 K because of the shorter unfolding time and significant fluctuation of the percentage of extended residues at 500 K.

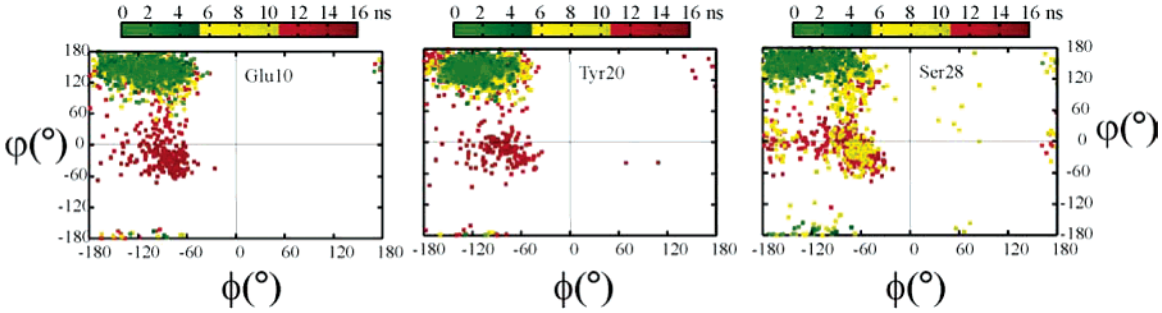

Figure 7. ϕ/φ distributions of the Glu10, Tyr20, and Ser28 residues of FBP28 in the simulation with explicit water solvent and the ff03 force field at 500 K. Glu10, Tyr20, and Ser28 are the middle residues of the first, the second, and the third strands in the native structure, respectively. The colors show the simulation time: beginning (green) to end (red).

behavior of FBP28 observed in experiments[22] and previous MD unfolding simulations with an explicit solvent model.[21] The transient nature of the helical content enabled the observation of a clear unfolding pathway: the persistence of the first two strands with the absence of the third strand and then the absence of all the strands in a predominant coiled structure. These results indicate that the ff03 force field has lower helix preference than the ff94 force field and a lower β-extended preference than the ff96 force field. The ff03 force field indeed has a better balance between α-helical and β-extended conformations than both ff94 and ff96, as stated in its reference paper.[4] We believe that the better balance comes from the new atomic charges as replacing the torsion parameters in ff94 with those in ff03 alone did not achieve such a result (see the blue lines in Figure 3).

At 500 K, unfolding was much quicker than at 430 K. The unfolding pathway was blurred by the significant fluctuation of the extended residues, and the helical content increased to more than 50% at ca. 2.4 ns (see the right-hand plot in Figure 5).

Despite the significant improvement of ff03 over ff94 and ff96, the overbiasing toward helical conformations still exists. To ensure that the effect of the implicit solvent model did not result in those biases, we conducted simulations with explicit water molecules for FBP28 at 430 K and 500 K. Figure 6 shows the time development of the percentage of residues in extended (solid line) and helical (dash line) conformations in a 45-ns trajectory at 430 K and a 16-ns trajectory at 500 K. The profiles are very similar to those with the NPSA model shown in Figure 5. Notable helical conformations are present in the trajectories but discontinuous until complete unfolding. After unfolding, helical conformations became the main population. Another similarity between simulations with the NPSA implicit solvent model and the explicit solvent model (Figures 6 and 5) is that the unfolding pathway is clearer at 430 K than at 500 K because of the shorter unfolding time and significant extended residue fluctuation at 500 K. Figure 7 shows the time development of the ϕ/φ distributions of the middle residues of the three native strands: Glu10, Tyr20, and Ser28, respectively, in the 500 K simulation. It is evident that all three residues converted from extended starting conformations to helical conformations at the end. The conversion of Ser28 in the third strand occurs earlier than that of Glu10 and Tyr20 in the first and the second strands. This is consistent with the lower stability of the third strand.

For comparison, we also conducted the same simulations for another WW domain, the YAP65 WW domain, which is less thermostable than FBP28.[18] The force field parameters in ff94, ff96, and ff03 showed similar effects for YAP65 and FBP28, although YAP65 exhibited less thermal stability by unfolding at lower temperatures (data not shown).

In addition, we simulated a 20-residue helical protein, the trp-cage miniprotein (PDB entry 1L2Y), with the NPSA implicit solvent model and the ff03 force field. The trp-cage protein folds into an α-helix and a short 3−10 helix with a

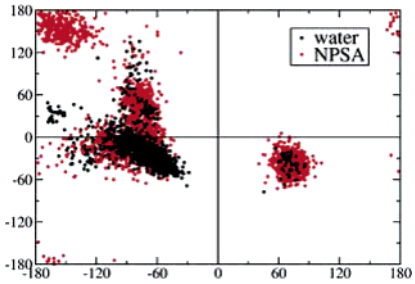

Figure 8. ϕ/φ distributions of the C-terminal residues Gln34, Glu35, and Leu36 of FBP28 in the simulations with the ff03 force field at 300 K. Black dots: with explicit water solvent; red dots: with $\sigma_{N\_bone} = -0.12$ kcal/mol·Å^2 in the NPSA model. The data for each model are from three 20-ns trajectories with different heating speeds to 300 K.

melting temperature of 42 degrees (315 K).[29] Our simulations were carried out at 5 different temperatures of 300 K, 315 K, 340 K, 370 K, and 500 K for 20 ns. At 300 K, both the secondary structure and the hydrophobic contacts between the residues in the trp cage were well maintained. Unfolding occurred on this time scale when the temperature was increased to 500 K, with the unstructured C-terminal segment separating from the helical N-terminal segment accompanied by the early loss of the short 3−10 helix. These results indicate that the reparametrized NPSA charges for the ff03 force field can maintain the protein native structures at room temperature and reproduce experimentally observed loss of structure at high temperatures for both β-sheet proteins and helical proteins.

We have investigated the effect of backbone torsion parameters in the context of the ff94 force field and the effect of the combination of backbone torsion parameters and atomic partial charges in the ff03 force field. The results demonstrated the superiority of the latter in terms of improving the balance between helical and extended conformations. Recently, Pande and co-workers[11] reported a result from the interplay between turning off the torsion potential, 1−4 charge−charge interactions and 1−4 van der Waals interactions for a helix-coil transition system. They found that the effects of these factors are complex being force-field dependent and nonadditive. This also implies that the improvement of empirical force fields is complex, and alteration of one parameter may require the modification of other parameters.

Solvation Parameter σ in the NPSA Model. Although there is no evidence to show that water plays a specific structural role in the folding/unfolding process of WW domains, the solvent properties and the treatment of solvent effects can affect the free energy landscape of folding/unfolding. Helical and extended conformations show different extents of solvent exposure. Explicitly including water molecules in a simulation is a natural and rigorous but computationally expensive way to account for solvent effects. Implicit solvent models use approximations to gain computational efficiency but suffer from less accuracy. When comparable results can be achieved, implicit solvent models are more attractive because of their high computational efficiency. For the 37-residue FBP28 WW domain, a 20-ns run on 4 Intel Pentium 4/2.4 GHz processors required 1.5 days with the NPSA implicit solvent model compared with 1 month with an explicit solvent model.

The solvent accessible surface area-dependent term in the NPSA model is designed to account implicitly for solvation effects. The solvation parameter σ can tune the extent of atomic exposure to solvent by being more negative for more exposure and more positive for more burial. Backbone nitrogen atoms are more exposed in a β-extended structure than in an α-helical structure. This means that setting a more negative solvation parameter σ to backbone nitrogen atoms might lead to stabilization of β-extended structures. We thus modified the solvation parameter σ_{N_bone} of backbone nitrogen atoms from the original −0.06 kcal/mol·Å^2 to −0.12 kcal/mol·Å^2. We first conducted 20-ns simulations at 300 K for three runs with different heating speeds. For comparison, we also conducted simulations with an explicit water model at 300 K. The three-stranded β-sheet native structure was maintained very well with both the explicit water model and the modified NPSA model. The only difference was in the C-terminal residues Gln34, Glu35, and Leu36. These three residues formed a stable non-native 3−10 helix in all three trajectories with the explicit water model, whereas they sampled both extended and helical conformations with the modified NPSA model. The ϕ/φ distributions of the three residues in the three trajectories of each model are shown in Figure 8. We can see that the three residues mainly sampled helical regions with the explicit solvent model, whereas, with the modified NPSA model, the three residues mainly sampled

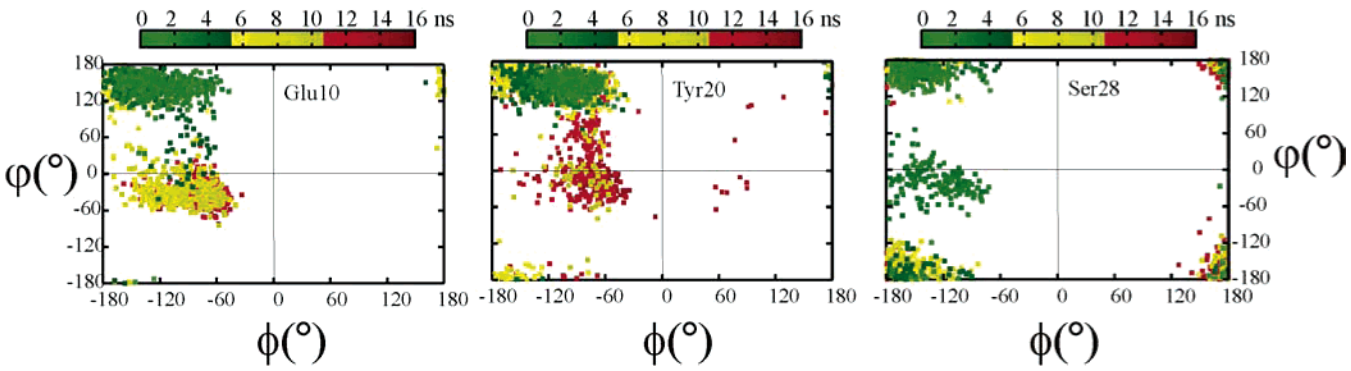

Figure 9. ϕ/φ distributions of the Glu10, Tyr20, and Ser28 residues of FBP28 in the simulation with $\sigma_{N\_bone} = -0.12$ kcal/mol·Å^2 in the NPSA model at 430 K. Glu10, Tyr20, and Ser28 are the middle residues of the first, the second, and the third strands in the native structure, respectively. The colors show the simulation time: beginning (green) to end (red).

the diagonal extended regions. In the NMR ensemble of 10 structures, the three C-terminal residues are either extended or coiled.

To investigate the performance of the modified NPSA model in unfolding simulations, we conducted 20-ns simulations at 430 K for three runs with different heating speeds. The three-stranded β-sheet native structure was lost in all three runs, and the remaining structural content was diverse with both non-native strands and helices existing. However, the loss of the native structure in the three runs did not exhibit an unfolding pathway consistent with experimental data. Figure 9 shows the time development of the ϕ/φ distributions of the middle residues Glu10, Tyr20, and Ser28 in the three native strands in one of the three 20-ns trajectories. The colors show the simulation time: beginning (green) to end (red). We can see that both Glu10 and Tyr20 moved to helical regions by the end of the simulation and Glu10 was faster than Tyr20 whereas Ser28 moved to corner extended regions. This reveals that the modified solvation parameter $\sigma_{N\_bone} = -0.12$ kcal/mol·Å^2 is not sufficient to prevent conversion to helical conformations and, at the same time, that the relative stabilities of the three strands were changed and became inconsistent with experimental data.

The lack of the expected improvement with the modified solvation parameter aiming at stabilizing extended conformations by increasing the solvent exposure of backbone nitrogen atoms indicates again that the intrinsic helix preference problem in AMBER force fields cannot be easily solved by refining a single parameter. In addition, we found that the modification of the solvation parameter in the NPSA model did not yield notable changes to the simulations for the helical trp-cage protein at both room temperature and higher temperatures. This indicates that the AMBER ff03 force field with the NPSA model is more robust for helical proteins than β-sheet proteins.

Conclusions

We have investigated several generations of the AMBER force field for simulation of a native 3-stranded β-sheet protein domain (along with several other small protein structures). The widely used ff94 force field and two backbone torsion potential variants were found to destabilize the β-sheet structure by directly converting it to an α-helix at high temperatures with the NPSA implicit solvent model. In contrast, the ff96 force field resulted in a highly elevated unfolding temperature and substantial non-native β-sheet structures with the NPSA implicit solvent model. These results are in agreement with previous studies revealing the helix-preference in the ff94 force field and the β-sheet preference in the ff96 force field with both an explicit solvent model and the generalized Born implicit solvent model. The newer ff03 force field showed much lower α-helix propensity compared to ff94 and lower β-strand propensity compared to ff96. More importantly, the ff03 force field allowed the observation of the experimentally observed unfolding pathway of the three-stranded β-sheet protein FBP28 with both the NPSA implicit solvent model and explicit water model. However, the ff03 force field still favors helical conformations in unfolded states. A modification of the solvation parameter of backbone nitrogen atoms in the NPSA model did not improve the results. This investigation also suggests that one should consider the integrative effects of all the force field parameters to improve the secondary structure balance of a force field.

Acknowledgment. The authors thank the Klaus Tschira Foundation for financial support and Dr. Peter J. Winn for critical reading of the paper.

Supporting Information Available: The full list of NPSA partial atomic charges. This material is available free of charge via the Internet at http://pubs.acs.org.

References

(1) Cornell, W. D.; Cieplak, P.; Bayly, C. I.; Gould, I. R.; Merz, K. M.; Ferguson, D. M.; Spellmeyer, D. C.; Fox, T.; Caldwell, J.; Kollman, P. A second generation of force field for the simulation of proteins, nucleic acids and organic molecules. *J. Am. Chem. Soc.* **1995**, *117*, 5179−5197.

(2) Kollman, P.; Dixon, R. W.; Cornell, W. D.; Fox, T.; Chipot, C.; Pohorille, A. The development/application of a 'minimalist' organic/biochemical molecular mechanic force field using a combination of ab initio calculations and experimental data. *Computer simulations of biological systems*; Escom: The Netherlands, 1997; pp 83−96.

(3) Wang, J.; Cieplak, P.; Kollman, P. How well does a restrained electrostatic potential (RESP) model perform in calculating conformational energies of organic and biological molecules? *J. Comput. Chem.* **2000**, *21*, 1049−1074.

(4) Duan, Y.; Wu, C.; Chowdhury, S.; Lee, M. C.; Xiong, G.; Zhang, W.; Yang, R.; Cieplak, P.; Luo, R.; Lee, T.; Caldwell, J.; Wang, J.; Kollman, P. A point-charge force field for molecular mechanics simulations of proteins based on condensed-phase quantum mechanical calculations. *J. Comput. Chem.* **2003**, *24*, 1999−2012.

(5) Neria, E.; Fischer, S.; Karplus, M. Simulation of activation free energies in molecular systems. *J. Chem. Phys.* **1996**, *105*, 1902−1921.

(6) MacKerell, A. D.; Bashford, D.; Bellott, M.; Dunbrack, R. L.; Evanseck, J. D.; Field, M. J.; Fischer, S.; Gao, J.; Guo, H.; Ha, S.; Joseph-McCarthy, D.; Kuchnir, L.; Kuczera, K.; Lau, F. T. K.; Mattos, C.; Michnick, S.; Ngo, T.; Nguyen, D. T.; Prodhom, B.; Reiher, W. E.; Roux, B.; Schlenkrich, M.; Smith, J. C.; Stote, R.; Straub, J.; Watanabe, M.; Wiorkiewicz-Kuczera, J.; Yin, D.; Karplus, M. All-Atom Empirical Potential for Molecular Modeling and Dynamics Studies of Proteins. *J. Phys. Chem. B* **1998**, *102*, 3586−3616.

(7) van Gunsteren, W. F.; Billeter, S. R.; Eising, A. A.; Huenenberger, P. H.; Krueger, P.; Mark, A. E.; Scott, W. R. P.; Tironi, I. G. *Biomolecular Simulation: The GROMOS Manual and User Guide*: Zuerich, 1996.

(8) Jorgensen, W. L.; Tirado-Rives, J. The OPLS [optimized potentials for liquid simulations] potential functions for proteins, energy minimizations for crystals of cyclic peptides and crambin. *J. Am. Chem. Soc.* **1988**, *110*, 1657−1666.

(9) Simmerling, C.; Strockbine, B.; Roitberg, A. E. All-atom structure prediction and folding simulations of a stable protein. *J. Am. Chem. Soc.* **2002**, *124*, 11258−11259.

(10) Garcia, A. E.; Sanbonmatsu, K. Y. α-helical stabilization by side chain shielding of backbone hydrogen bonds. *Proc. Natl. Acad. Sci.* **2002**, *99*, 2782−2787.

(11) Sorin, E. J.; Pande, V. S. Empirical force-field assessment: The interplay between backbone torsions and noncovalent term scaling. *J. Comput. Chem.* **2005**, *26*, 682−690.

(12) Beachy, M.; Chasman, D.; Murphy, R.; Halgren, T.; Friesner, R. Accurate ab initio quantum chemical determination of the relative energetics of peptide conformations and assessment of empirical force fields. *J. Am. Chem. Soc.* **1997**, *119*, 5908−5920.

(13) Gnanakaran, S.; Garcia, A. E. Helix-coil transition of alanine peptides in water: force field dependence on the folded and unfolded structures. *Proteins* **2005**, *59*, 773−782.

(14) Zhou, R.; Berne, B. J. Can a continuum solvent model reproduce the free energy landscape of a beta -hairpin folding in water? *Proc. Natl. Acad. Sci.* **2002**, *99*, 12777−12782.

(15) Okur, A.; Strockbine, B.; Hornak, V.; Simmerling, C. Using PC clusters to evaluate the transferability of molecular mechanics force fields for proteins. *J. Comput. Chem.* **2003**, *24*, 21−31.

(16) Sorin, E. J.; Pande, V. S. Exploring the helix-coil transition via all-atom equilibrium ensemble simulations. *Biophys. J.* **2005**, *88*, 2472−2493.

(17) Wang, T.; Wade, R. C. Implicit solvent models for flexible protein−protein docking by molecular dynamics simulation. *Proteins* **2003**, *50*, 158−169.

(18) Ferguson, N.; Johnson, C. M.; Macias, M.; Oschkinat, H.; Fersht, A. Ultrafast folding of WW domains without structured aromatic clusters in the denatured state. *Proc. Natl. Acad. Sci.* **2001**, *98*, 13002−13007.

(19) Crane, J. C.; Koepf, E. K.; Kelly, J. W.; Gruebele, M. Mapping the transition state of the WW domain beta-sheet. *J. Mol. Biol.* **2000**, *298*, 283−292.

(20) Jaeger, M.; Nguyen, H.; Crane, J. C.; Kelly, J. W.; Gruebele, M. The folding mechanism of a beta-sheet: The WW domain. *J. Mol. Biol.* **2001**, *311*, 373−393.

(21) Ferguson, N.; Pires, J. R.; Toepert, F.; Johnson, C. M.; Pan, Y.-P.; Volkmer-Engert, R.; Schneider-Mergener, J.; Daggett, V.; Oschkinat, H.; Fersht, A. Using flexible loop mimetics to extend phi-value analysis to secondary structure interactions. *Proc. Natl. Acad. Sci.* **2001**, *98*, 13008−13013.

(22) Nguyen, H.; Jager, M.; Moretto, A.; Gruebele, M.; Kelly, J. W. Tuning the free-energy landscape of a WW domain by temperature, mutation, and truncation. *Proc. Natl. Acad. Sci.* **2003**, *100*, 3948−3953.

(23) Nymeyer, H.; Garcia, A. E. Simulation of the folding equilibrium of alpha-helical peptides: a comparison of the generalized Born approximation with explicit solvent. *Proc. Natl. Acad. Sci.* **2003**, *100*, 13934−13939.

(24) Ono, S.; Nakajima, N.; Higo, J.; Nakamura, H. Peptide free-energy profile is strongly dependent on the force field: Comparison of C96 and AMBER95. *J. Comput. Chem.* **2002**, *21*, 748−762.

(25) Frishman, D.; Argos, P. Knowledge-based protein secondary structure assignment. *Proteins* **1995**, *23*, 566−579.

(26) Humphrey, W.; Dalke, A.; Schulten, K. VMD: visual molecular dynamics. *J. Mol. Graph.* **1996**, *14*, 33−38, 27−38.

(27) Munoz, V.; Serrano, L. Elucidating the folding problem of helical peptides using empirical parameters. *Nat. Struct. Biol.* **1994**, *1*, 399−409.

(28) Rost, B. PHD: predicting one-dimensional protein structure by profile based on neural networks. *Methods Enzymol.* **1996**, *266*, 525−539.

(29) Neidigh, J. W.; Fesinmeyer, R. M.; Andersen, N. H. Designing a 20-residue protein. *Nat. Struct. Biol.* **2002**, *9*, 425−430.

CT0501607